Please cite this article in press as: Huh et al., Age- and Pregnancy-Associated DNA Methylation Changes in Mammary Epithelial Cells, Stem Cell Reports (2015), http://dx.doi.org/10.1016/j.stemcr.2014.12.009

Stem Cell Reports
Article
ISSCR
OPEN ACCESS

Age- and Pregnancy-Associated DNA Methylation Changes in Mammary Epithelial Cells

Sung Jin Huh,[1,2,3,13] Kendell Clement,[4,5,6,7,13] David Jee,[1,2,3] Alessandra Merlini,[1,8] Sibgat Choudhury,[1,2,3] Reo Maruyama,[1,2,3] Ronnie Yoo,[9,10] Anna Chytil,[11] Patrick Boyle,[4] Fei Ann Ran,[9,10] Harold L. Moses,[11] Mary Helen Barcellos-Hoff,[12] Laurie Jackson-Grusby,[6,9,10] Alexander Meissner,[4,5,6,*] and Kornelia Polyak[1,2,3,4,6,9,*]

[1]Department of Medical Oncology, Dana-Farber Cancer Institute, Boston, MA 02215, USA
[2]Department of Medicine, Brigham and Women's Hospital, Boston, MA 02115, USA
[3]Department of Medicine, Harvard Medical School, Boston, MA 02115, USA
[4]Broad Institute of MIT and Harvard, Cambridge, MA 02142, USA
[5]Department of Stem Cell and Regenerative Biology, Harvard University, Cambridge, MA 02138, USA
[6]Harvard Stem Cell Institute, Cambridge, MA 02138, USA
[7]Harvard-MIT Division of Health Sciences and Technology, Cambridge, MA 02139, USA
[8]Unit of Immunology and General Pathology, Department of Molecular Medicine, University of Pavia, 27100 Pavia, Italy
[9]Program in Biological and Biomedical Sciences, Harvard Medical School, Boston, MA 02115, USA
[10]Department of Pathology, Children's Hospital Boston, Boston, MA 02115, USA
[11]Department of Cancer Biology and Vanderbilt-Ingram Cancer Center, Vanderbilt University School of Medicine, Nashville, TN 37232, USA
[12]Departments of Radiation Oncology and Cell Biology, New York University School of Medicine, New York, NY 10016, USA
[13]Co-first author
*Correspondence: alexander_meissner@harvard.edu (A.M.), kornelia_polyak@dfci.harvard.edu (K.P.)
http://dx.doi.org/10.1016/j.stemcr.2014.12.009

SUMMARY

Postnatal mammary gland development and differentiation occur during puberty and pregnancy. To explore the role of DNA methylation in these processes, we determined the genome-wide DNA methylation and gene expression profiles of $CD24^{+}CD61^{+}CD29^{hi}$, $CD24^{+}CD61^{+}CD29^{lo}$, and $CD24^{+}CD61^{-}CD29^{lo}$ cell populations that were previously associated with distinct biological properties at different ages and reproductive stages. We found that pregnancy had the most significant effects on $CD24^{+}CD61^{+}CD29^{hi}$ and $CD24^{+}CD61^{+}CD29^{lo}$ cells, inducing distinct epigenetic states that were maintained through life. Integrated analysis of gene expression, DNA methylation, and histone modification profiles revealed cell-type- and reproductive-stage-specific changes. We identified p27 and TGFβ signaling as key regulators of $CD24^{+}CD61^{+}CD29^{lo}$ cell proliferation, based on their expression patterns and results from mammary gland explant cultures. Our results suggest that relatively minor changes in DNA methylation occur during luminal differentiation compared with the effects of pregnancy on $CD24^{+}CD61^{+}CD29^{hi}$ and $CD24^{+}CD61^{+}CD29^{lo}$ cells.

INTRODUCTION

The mammary gland is a unique organ because its functional development and differentiation are completed postnatally. Ductal branching and elongation take place during puberty, whereas lobulo-alveolar development and differentiation into milk-secreting alveoli occur during pregnancy and lactation (Hennighausen and Robinson, 2005). The mammary ducts are composed of the outer contractile myoepithelial cells and the inner luminal epithelial cells. These two main epithelial lineages originate from bipotential mammary epithelial stem cells (MaSCs) during embryonic development, and in postnatal life they may be maintained by lineage-committed progenitors, with bipotential stem cells playing a lesser role under physiologic conditions (Rios et al., 2014; Shackleton et al., 2006; Spike et al., 2012; Van Keymeulen et al., 2011). In vivo lineage tracing and mammary transplant studies regarding the relative role of bipotential stem cells and committed progenitors in the maintenance of adult mammary glands have been controversial (Prater et al., 2014; Rios et al., 2014; Shackleton et al., 2006; Van Keymeulen et al., 2011), likely due to the different experimental conditions used and the relative plasticity of mammary epithelial progenitors (van Amerongen et al., 2012). The cell-surface markers CD24, CD29, and CD61 have been identified in multiple strains of mice as markers of three distinct mammary epithelial populations enriched for MaSCs, but they also contain myoepithelial and other basal cells ($CD24^{+}CD61^{+}CD29^{hi}$), luminal progenitors ($CD24^{+}CD61^{+}CD29^{lo}$), and mature luminal epithelial cells ($CD24^{+}CD61^{-}CD29^{lo}$) (Asselin-Labat et al., 2007; Desgrosellier et al., 2014; Gu et al., 2013; Shackleton et al., 2006). $CD24^{+}CD61^{+}CD29^{hi}$ cells can give rise to both myoepithelial and luminal lineages in mammary transplant assays, whereas $CD24^{+}CD61^{+}CD29^{lo}$ cells can only produce mature luminal cells (Asselin-Labat et al., 2007; Prater et al., 2014).

Cellular differentiation is governed by epigenetic programs such as DNA methylation and chromatin modification (Smith and Meissner, 2013). The requirement for

DNA methylation in early embryonic development has been demonstrated by the phenotype of DNA methyltransferase (DNMT) knockout mouse models in which homozygous deletion of *Dnmt1*, *Dnmt3a*, or *Dnmt3b* leads to early embryonic or postnatal lethality (Smith and Meissner, 2013). DNMTs are also required for embryonic stem cell (ESC) differentiation (Smith and Meissner, 2013). Changes in DNA methylation and histone modification patterns are clearly associated with the differentiation of normal adult tissue-specific stem cells (Smith and Meissner, 2013), but their relevance for cell-type-specific expression patterns has not been investigated.

Here, we describe the comprehensive molecular profiling of three distinct mammary epithelial cell types ($CD24^+CD61^+CD29^{hi}$, $CD24^+CD61^+CD29^{lo}$, and $CD24^+CD61^-CD29^{lo}$) from C57BL6 female mice of different ages and reproductive stages. We also analyzed the effects of DNMT inhibitors and genetic depletion of *Dnmt1* by analyzing mammary glands from 5-azacytidine (AzaC)-treated and $Dnmt1^{+/chip}$ hypomorphic mice (Gaudet et al., 2003), respectively.

RESULTS

Differences in Mammary Gland Morphology and Cellular Composition Related to Age, Reproductive Stage, and DNMT Activity

To establish the normal mammary epithelial states at different ages and reproductive stages, we first examined the mammary gland morphology and the relative fraction of three distinct cell populations defined by fluorescence-activated cell sorting (FACS) in pre- and postpubertal and old virgin (3, 9, and 24 weeks old, respectively), early and late pregnant (day 10 [D10], D16, and D19), and retired breeder (28–36 weeks old, $\geq$5 pregnancies/mouse) C57/BL6 female mice (Figures 1A–1C; Table S1 available online). Despite the fact that the mammary gland remodels to a virgin-like state after pregnancy, the mammary glands of retired breeders had more tertiary branching compared with 9-week-old virgins, and the mammary glands of 24-week-old virgins were morphologically the most similar to the 9-week-old virgin glands (Figure 1A).

The relative frequencies of $CD24^+CD61^+CD29^{hi}$, $CD24^+CD61^+CD29^{lo}$, and $CD24^+CD61^-CD29^{lo}$ cells were determined by FACS (Desgrosellier et al., 2014; Gu et al., 2013). Similar to previous findings (Desgrosellier et al., 2014), the most significant differences were observed in the relative fraction of $CD24^+CD61^+CD29^{lo}$ cells, with a gradual decline in 3–9- to 24-week-old virgins. The lowest levels were found in pregnant mice, followed by a return to 9-week-old virgin levels in retired breeders (Figures 1B and 1C). However, due to the larger absolute number of mammary epithelial cells in pregnant mice, this relative decline during pregnancy may not reflect a decrease in the absolute numbers of these cells. The relative frequency of $CD24^+CD61^-CD29^{lo}$ cells gradually increased during pregnancy and returned to prepuberty levels in retired breeders. Interestingly, the effects of aging on the frequency of $CD24^+CD61^+CD29^{hi}$ and $CD24^+CD61^+CD29^{lo}$ cells were similar to those of pregnancy, since the 24-week-old virgin values were in between the 9-week-old virgin and D10 pregnant levels (Figure 1C).

Next, we investigated the role of DNMT activity in ductal development (virgin mice) and in alveogenesis (pregnant mice) by using azacitidine (AzaC) DNMT inhibitor (Figure S1A). We also tested the effects of valproic acid (VPA), a histone deacetylase (HDAC) inhibitor, since it has been shown to promote cellular differentiation in other systems (Tou et al., 2004). The efficacy of AzaC treatment was confirmed by analysis of DNA methylation of SINE B1 elements (Kramerov and Vassetzky, 2005) and the expression of genes silenced by DNA methylation (Figures S1B and S1C). We found that the overall size and extent of ductal/alveolar structures decreased significantly in AzaC-treated mice compared with control mice, whereas no differences were seen in VPA-treated animals (Figures 1D and 1E). The relative fractions of $CD24^+CD61^+CD29^{hi}$ and $CD24^+CD61^+CD29^{lo}$ did not change significantly upon either AzaC or VPA treatment in virgin mice (Figure 1F). In contrast, there was a small but significant decrease of $CD24^+CD61^+CD29^{hi}$ cells in VPA-treated pregnant animals, and both drugs induced a slight but significant increase in the representation of $CD24^+CD61^-CD29^{lo}$ cells in both virgin and pregnant mice. Thus, the observed morphologic changes in AzaC-treated animals were more likely due to decreased cell proliferation and an overall decrease in mammary epithelial cells rather than to specific effects on any cell type (Figure 1F).

Since AzaC treatment may have indirect effects, we analyzed the mammary gland morphology and cellular composition in $Dnmt1^{+/chip}$ (heterozygous Dnmt1 hypomorph) mice to directly address the role of Dnmt1 and DNA methylation in mammary gland development (Figures 1G and 1H). In this mouse model, an ~55% decrease of Dnmt1 expression was associated with a slight increase in the relative representation of $CD24^+CD61^+CD29^{hi}$ cells and a slight decrease of $CD24^+CD61^+CD29^{lo}$ cells compared with wild-type (WT)/WT 9-week-old virgin mice, but neither change was significant. Unfortunately, we were not able to characterize $Dnmt1^{+/chip}$ mice during pregnancy, where the changes might be more pronounced, due to difficulties with breeding these animals.

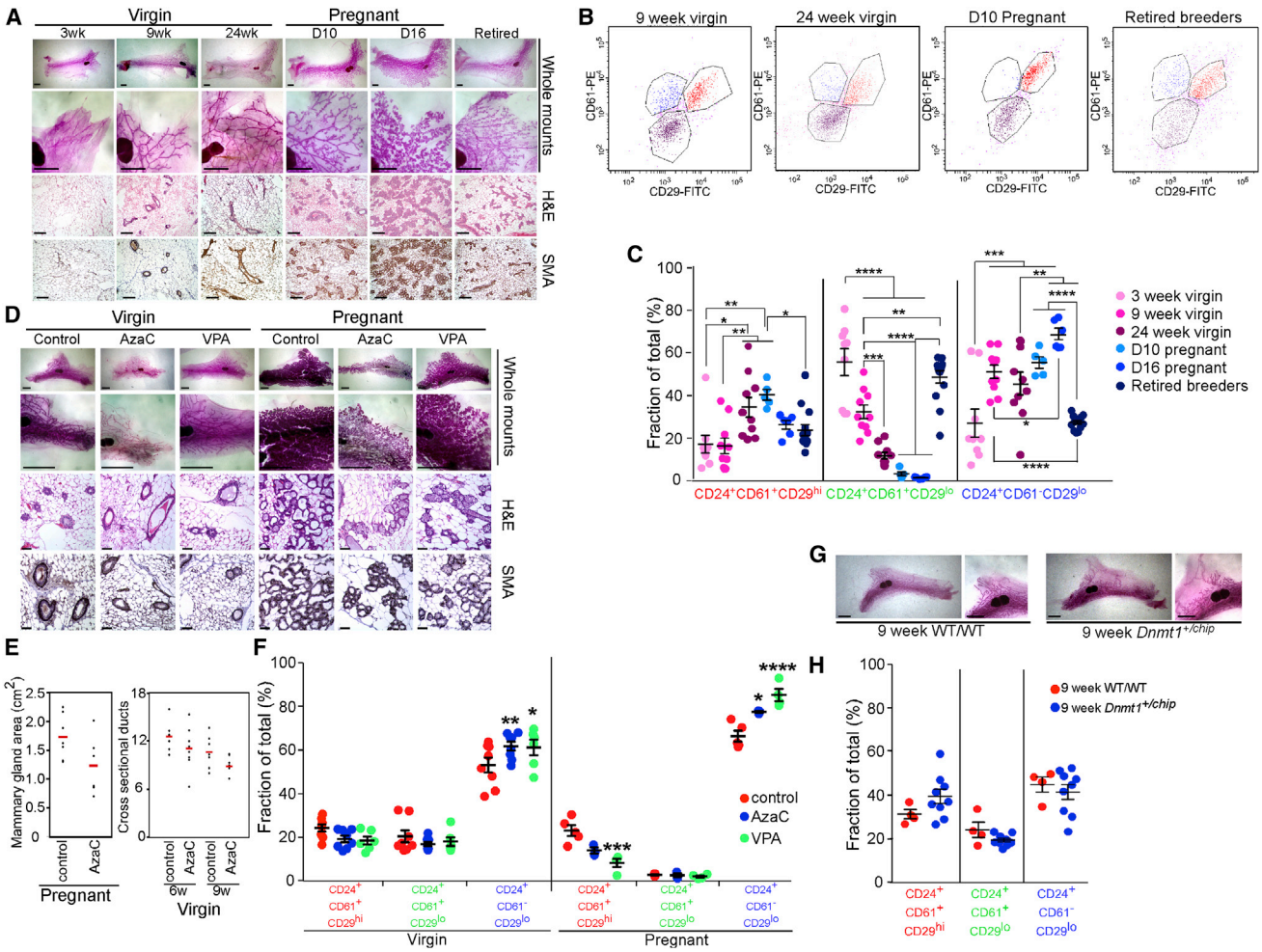

Figure 1. Changes in the Mammary Epithelium Associated with Age, Reproductive Stage, and AzaC Treatment

(A) Morphology of mouse mammary glands at different age and reproductive stages by whole-mount (top; scale bar, 2.5 mm), H&E (middle; scale bar, 50 μm), and smooth muscle actin (SMA, bottom; scale bar, 50 μm) staining.

(B and C) Representative FACS profiles (B) and graph (C) depicting the relative frequencies of the indicated cell populations at the specified age and reproductive stages. Asterisks indicate significant differences (*$p < 0.05$, **$p < 0.005$, ***$p < 0.001$, ****$p < 0.0001$; two-way ANOVA, Tukey's multiple-comparison test). Error bars represent median ± SEM.

(D) Morphologic changes induced by AzaC and VPA treatment based on whole-mount (top; scale bar, 2.5 mm), H&E (middle; scale bar, 50 μm), and SMA (bottom; scale bar 50 μm) staining.

(E) AzaC-treatment-induced changes in mammary gland size and ductal branching (assessed by the number of cross-sectional ducts) in pregnant and virgin mice, respectively. Inset shows representative mammary glands from control and AzaC-treated pregnant mice.

(F) Relative fraction of $CD61^+CD29^{hi}$, $CD24^+CD61^+CD29^{lo}$, and $CD24^+CD^{61-}CD29^{lo}$ cells in AzaC- or VPA-treated mice. Asterisks indicate significant differences (*$p < 0.05$, **$p < 0.005$, ***$p < 0.001$, ****$p < 0.0001$; two-way ANOVA, Dunnett's multiple-comparison test) between PBS control and AzaC- or VPA-treated groups within each cell type. Error bars represent median ± SEM.

(G) Whole mounts of mouse mammary glands from *Dnmt1*$^{+/chip}$ mice. Scale bar, 2.5 mm.

(H) Relative fraction of $CD61^+CD29^{hi}$, $CD24^+CD61^+CD29^{lo}$, and $CD24^+CD^{61-}CD29^{lo}$ cells in 9-week-old virgin *Dnmt1*$^{+/chip}$ mice. Error bars represent median ± SEM.

See also Figure S1 and Table S1.

Cell-type and Reproductive-Stage-Specific Gene Expression Patterns

To define molecular differences among the three cell types at different ages and reproductive stages, we analyzed the gene expression profiles of each cell population from multiple independent mice (pools of cells from 36–108 mice depending on the developmental stage). This analysis revealed significant cell-type-, age-, and

reproductive-stage-specific differences, with the clearest separation of $CD24^+CD61^+CD29^{hi}$ cells from the other two cell types, and pregnant samples from all others (Figures 2A and 2B). Age and reproductive stage had the most pronounced effects on the profiles of $CD24^+CD61^+CD29^{hi}$ and $CD24^+CD61^+CD29^{lo}$ cells (Figure 2B; Tables S2 and S3), correlating with our data in humans (Choudhury et al., 2013). Several genes involved in growth factor signaling (e.g., *Igf2r*) were highly expressed in $CD24^+CD61^+CD29^{lo}$ cells of 3- to 9-week-old virgin mice but decreased in old virgin, pregnant, and retired breeders. In contrast, genes related to milk production (e.g., *Csna*) and lactation (e.g., *Oxtr*) were highly expressed in $CD24^+CD61^+CD29^{lo}$ and $CD24^+CD61^-CD29^{lo}$ cells of pregnant mice.

Next, we analyzed the relative differences in gene expression between cell types at different stages and stage-specific differences within the same cell type (Table S4). These analyses provided evidence of luminal differentiation and highlighted the distinct transcriptional state during pregnancy (Figure 2C). Although $CD24^+CD61^+CD29^{lo}$ and $CD24^+CD61^-CD29^{lo}$ cells had correlated transcription in virgin and retired breeder mice, a decrease in correlation during pregnancy showed the activation of unique expression programs. Further analysis of genes with the most significant differences according to cell type and developmental stage revealed enrichment in distinct biological functions. Development-related genes were specific to and highly expressed in $CD24^+CD61^+CD29^{hi}$ and $CD24^+CD61^+CD29^{lo}$ cells in all stages (Figures 2D and 2E; Tables S2 and S3). In young virgin mice, $CD24^+CD61^-CD29^{lo}$ cells displayed a significant overlap with $CD24^+CD61^+CD29^{lo}$ cells, thus implying that full luminal maturation may not occur until after pregnancy. In pregnant mice, lactation was a top functional category in $CD24^+CD61^-CD29^{lo}$ cells, correlating with lactation-associated changes during pregnancy. Some pathways were significantly enriched in multiple pairwise comparisons (Figure S2A). For example, neuroactive ligand-receptor interactions were highly represented in changes observed in both $CD24^+CD61^+CD29^{hi}$ and $CD24^+CD61^+CD29^{lo}$ cells due to age and reproductive stage, although the actual genes varied (Table S5).

Because transcription factors (TFs) are key regulators of cellular phenotypes, we investigated their expression patterns in more detail. We found that the expression of many TFs known to be required for mammary gland development and differentiation was restricted to a specific cell type and developmental stage. For example, *Elf5* and *Stat5*, which have known roles in alveolar differentiation and lactation, were most highly expressed in $CD24^+CD61^+CD29^{lo}$ and $CD24^+CD61^-CD29^{lo}$ cells of pregnant mice, whereas *Foxa1* and *Esr1* luminal genes had the highest expression in $CD24^+CD61^+CD29^{lo}$ cells of young virgin mice (Figures 2F and S2B). $CD24^+CD61^+CD29^{hi}$ cells had the highest number of unique TFs, including several members of the *Id*, *Snai*, and *Foxo* families (Figures 2G–2I). *Id4* and *Snai2* were specifically expressed in $CD24^+CD61^+CD29^{hi}$ cells regardless of age and reproductive stage (Figure 2G), whereas *Snai1* was relatively specific to $CD24^+CD61^+CD29^{hi}$ and $CD24^+CD61^+CD29^{lo}$ cells from young virgin mice, and *Foxd3* and *Foxa3* were relatively specific to those from pregnant and retired breeder mice (Figure 2H). *Snai1* can cooperate with *Sox9* to induce MaSCs (Guo et al., 2012). *Foxd3* is essential for ESCs and for maintaining pluripotent cells during embryonic development (Hanna et al., 2002). Thus, the high expression of these TFs in the $CD24^+CD61^+CD29^{hi}$ cell fraction is consistent with a functional role in stem cells.

Cell-Type-Specific and Pregnancy-Induced Changes in DNA Methylation Patterns

Next, we analyzed the global DNA methylation profiles of each cell type at all ages and reproductive stages using reduced representation bisulfite sequencing (RRBS) (Boyle et al., 2012). The global methylation signature of these mammary epithelial cell populations is more closely related to that of skin than to that of blood (Bock et al., 2012; Figure 3A), which is in agreement with its developmental origin. In contrast to the relatively large difference among blood, skin, and mammary samples based on Pearson correlation, the DNA methylation profiles of the mammary epithelial cell types were relatively similar. Nonetheless, global (Figure S2C) as well as promoter and enhancer DNA methylation signatures (Figures 3B and 3C) varied more between cellular states than between reproductive states. However, contrary to the clustering of samples based on expression data in which all $CD24^+CD61^+CD29^{hi}$ cells cluster together, the DNA methylation data highlighted a unique cluster that contained only the $CD24^+CD61^+CD29^{hi}$ cells from old virgin, pregnant, and retired breeder mice (Figures 3B and 3C). These results suggest that aging and pregnancy may permanently alter the DNA methylation profiles of $CD24^+CD61^+CD29^{hi}$ cells. Nevertheless, since the $CD24^+CD61^+CD29^{hi}$ cell fraction is composed of multiple cell types, the observed differences in molecular profiles might be influenced by changes in the biological composition of this phenotypically defined population.

The majority of promoters did not show significant DNA methylation changes across cell type (n = 15,395) or developmental stage (n = 15,362), in agreement with prior studies in other organs (Bock et al., 2012; Ziller et al., 2013). However, in both groups we found a select number of interesting genes that showed altered promoter DNA methylation patterns. For instance, 107 and 48 loci displayed increased and decreased DNA methylation

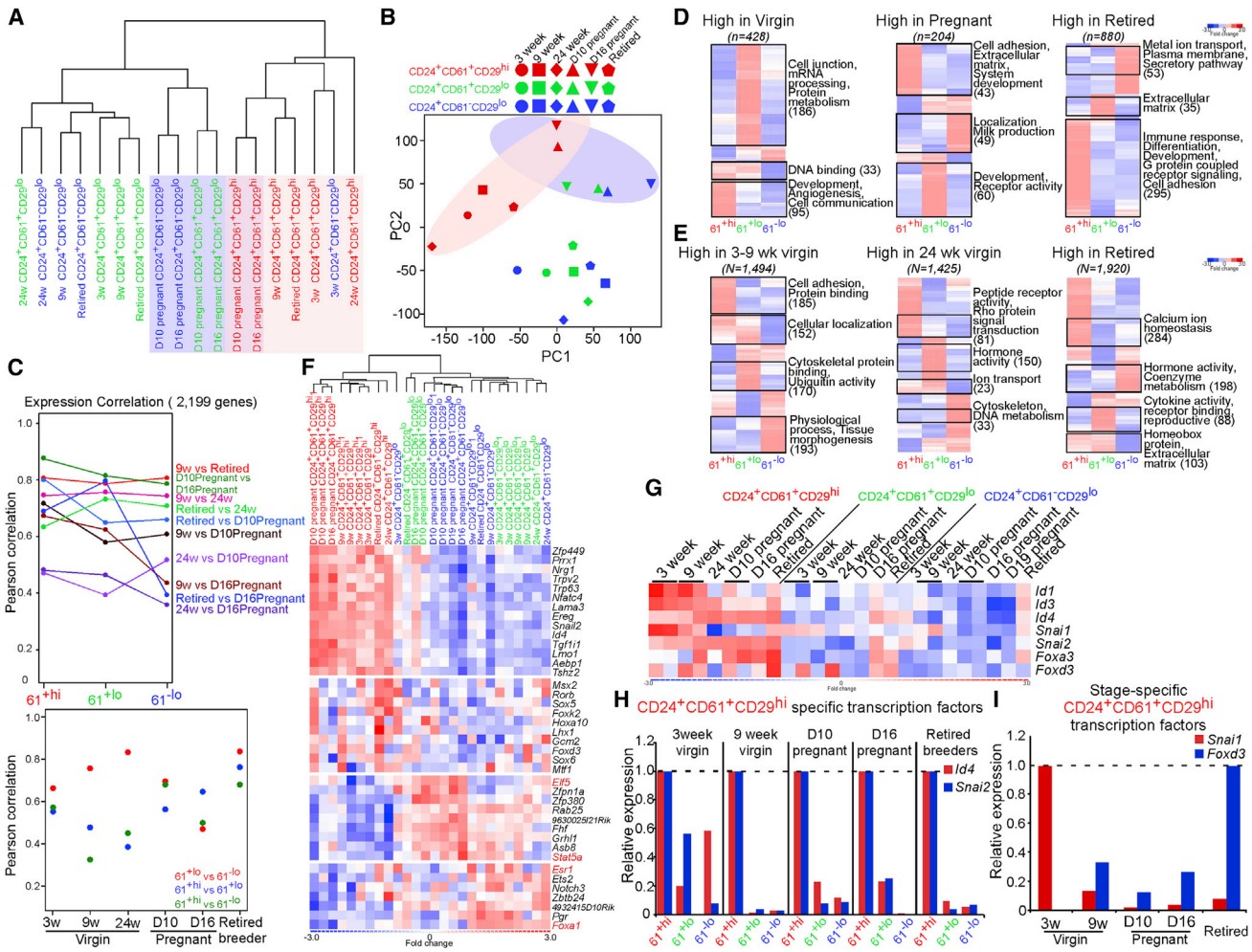

Figure 2. Changes in Gene Expression Patterns in the Mammary Epithelium Specific to Cell Type, Age, and Reproductive Stage

(A) Unsupervised hierarchical clustering of mammary epithelial gene expression profiles based on all expressed genes.

(B) 2D projection of the gene expression data onto the first two principal components. Cell types and reproductive stages are indicated by colors and shapes, respectively.

(C) Top: correlation plot of each cell type in two different developmental stages using the top 10% differential expressed genes. Bottom: correlation plot of cell types within each developmental stage using the top 10% differential expressed genes. See also Table S4.

(D) Heatmaps depicting genes differentially expressed among cell types in 3- to 9-week-old virgin, pregnant, and retired breeder mice. Green rectangles highlight cell-type-specific genes, with prominent functional categories indicated. 61^{+hi} (red), 61^{+lo} (green), and 61^{-lo} (blue) indicate $CD24^{+}CD61^{+}CD29^{hi}$, $CD24^{+}CD61^{+}CD29^{lo}$, and $CD24^{+}CD61^{-}CD29^{lo}$, respectively. See also Table S2.

(E) Heatmaps depicting genes differentially expressed among cell types in 3- to 9-week-old virgin, 24-week-old virgin, and retired breeder mice. Green rectangles highlight cell-type-specific genes, with prominent functional categories indicated. 61^{+hi} (red), 61^{+lo} (green), and 61^{-lo} (blue) indicate $CD24^{+}CD61^{+}CD29^{hi}$, $CD24^{+}CD61^{+}CD29^{lo}$, and $CD24^{+}CD61^{-}CD29^{lo}$, respectively. See also Table S3.

(F) Heatmap depicting clustering of the samples based on the mRNA levels of TFs differentially expressed between cell types and reproductive stages. TFs with known roles in mammary gland development are highlighted in red.

(G) Heatmap depicting mRNA levels of selected TFs differentially expressed in $CD24^{+}CD61^{+}CD29^{hi}$ cells according to age and reproductive stage.

(H and I) qRT-PCR validation of the expression of selected TFs that were highly expressed in $CD24^{+}CD61^{+}CD29^{hi}$ cells regardless of reproductive status (H) or at a specific stage (I). 61^{+hi} (red), 61^{+lo} (green), and 61^{-lo} (blue) indicate $CD24^{+}CD61^{+}CD29^{hi}$, $CD24^{+}CD61^{+}CD29^{lo}$, and $CD24^{+}CD61^{-}CD29^{lo}$, respectively.

See also Figure S2.

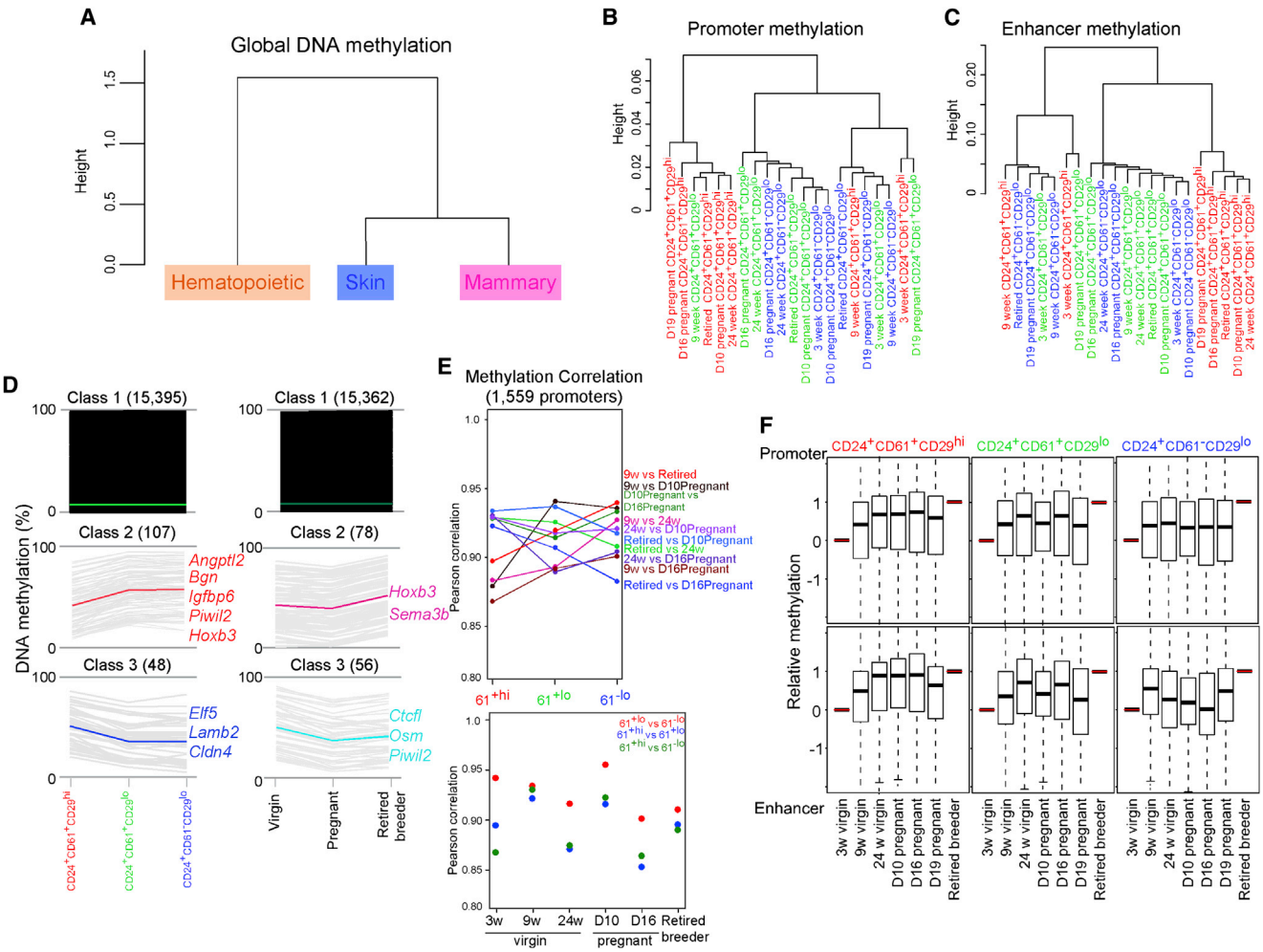

Figure 3. Changes in DNA Methylation Patterns in the Mammary Epithelium Specific to Cell Type, Age, and Reproductive Stage

(A) Clustering of different cell types from skin, blood, and mammary gland using Ward's method of Pearson correlations between individual CpGs that were present in each pairwise comparison with coverage of five or more reads.

(B and C) Hierarchical clustering based on the mean DNA methylation in promoter (B) and enhancer (C) regions.

(D) Changes in promoter DNA methylation between cell types (left) and reproductive stages (right) are separated into classes of genes that show no change, increase, or decrease in DNA methylation. Selected genes with known functions in stem cells or mammary gland development are listed.

(E) Top: correlation plot of each cell type in two different developmental stages using the top 10% differential methylated genes. Bottom: correlation plot of cell types within each developmental stage using the top 10% differential methylated genes. 61^{+hi} (red), 61^{+lo} (green), and 61^{-lo} (blue) indicate $CD24^{+}CD61^{+}CD29^{hi}$, $CD24^{+}CD61^{+}CD29^{lo}$, and $CD24^{+}CD61^{-}CD29^{lo}$, respectively.

(F) Comparison of promoter and enhancer DNA methylation of each cell type at different age and reproductive stages. For each gene, the initial 3w virgin methylation level was set to 0, and the final retired level was set to 1. At each intermediate stage, the methylation level for that stage was normalized as a proportion of the absolute change between the initial 3-week-old virgin and the final retired methylation level. The boxplot summarizes the relative methylation values for each gene. The bar shows the median value and the box shows the inner quartile range, with whiskers (which extend beyond the plot edges) showing the range of data values.

See also Figures S2 and S3 and Tables S4, S6, and S7.

levels, respectively, in $CD24^{+}CD61^{+}CD29^{lo}$ cells, and these remained at approximately the same levels in $CD24^{+}CD61^{-}CD29^{lo}$ cells (Figures 3D and S2D; Table S6). Genes that were hypermethylated in $CD24^{+}CD61^{+}CD29^{lo}$ and $CD24^{+}CD61^{-}CD29^{lo}$ cells included stem-cell-related genes (e.g., *Angptl2*), whereas many hypomethylated genes were related to epithelial cell differentiation (e.g., *Elf5* and *Cldn4*). Similarly, 78 genes gained and 56 genes lost promoter DNA methylation in all cells from retired breeder mice compared with those from virgin and pregnant

animals (Figure 3D). Several of these genes have known oncogenic (e.g., *Hoxb3*) (Li et al., 2012) or tumor-suppressive (e.g., *Ctcfl*) (Tiffen et al., 2013) functions in breast cancer. The expression and promoter DNA methylation of class 2 and 3 genes in different cell types and reproductive stages clearly showed a reverse correlation, suggesting that changes in promoter DNA methylation play a role in regulating gene expression (Figure S2E). We performed a functional classification of genes in each class of Figure 3D, but the relatively low number of genes did not reveal enrichment for significant biological functions. However, there was some overlap in the functional terms characterizing differentially expressed and differentially methylated genes, including "tissue development" and "DNA binding."

Next, we analyzed the relative differences in DNA methylation between cell types at different stages as well as stage-specific differences within the same cell type. Unlike expression, for which cells developed specific transcriptional identities with cell-type maturation, the DNA methylation landscape appeared to vary most with the progression of reproductive stages, with a gradual decrease in correlation between DNA methylation states going from virgin to pregnant to retired breeder mice (Figure 3E; Table S4).

To further explore pregnancy-induced and persistent methylation changes, we compared the DNA methylation values for all stages relative to the initial (week 3) and final (retired breeder) stages (Figure 3F). $CD24^{+}CD61^{+}CD29^{hi}$ showed a gradual trend toward retired breeder values from puberty through aging and pregnancy in both promoter and enhancer methylation, and these values were maintained through late pregnancy and postpregnancy stages. These results provided further evidence that aging and pregnancy are associated with persistent DNA methylation changes in $CD24^{+}CD61^{+}CD29^{hi}$ and $CD24^{+}CD61^{+}CD29^{lo}$ cells, whereas the DNA methylation patterns of $CD24^{+}CD61^{-}CD29^{lo}$ cells are stable. Despite the relatively similar trend in the degree of DNA methylation in old virgin and pregnant mice, the actual identities of the genes that showed these changes were different: lowly expressed genes were preferentially hypermethylated due to age, but not to pregnancy. This is similar to previous findings in blood, which showed that silent genes were targets for aberrant age-related silencing (Beerman et al., 2013).

To further investigate core signatures characterizing pregnancy-induced and persistent methylation changes, we analyzed the top 10% of genes that had differential DNA methylation in the promoters or enhancers between 3-week-old virgin and retired breeders, and remained between 50% and 150% in the pregnant mice (Figure S2E). Several genes with pregnancy-induced and persistent DNA methylation changes have known roles in mammary gland development (e.g., *Wnt3*) or breast tumorigenesis (e.g., *Hs3st2* and *Trim29*) (Table S7).

We also analyzed the gene expression profiles of mammary glands from mice treated with AzaC or VPA. Treatment with these agents induced more pronounced effects on gene expression in pregnant mice, potentially due to the higher fraction of proliferative cells that were more responsive to epigenetic drugs (Figure S3A). Interestingly, almost all genes with a change in expression were altered in the same way by both AzaC and VPA. Consistent with decreased cell proliferation, both AzaC and VPA treatment decreased cyclin D1 (*Ccnd1*) expression. Additionally, most genes induced by these treatments did not show cell-type or developmental-stage-specific expression or methylation changes, with the exception of a handful of AzaC-induced genes (e.g., *Cldn4*) that were differentially expressed and methylated between $CD24^{+}CD61^{+}CD29^{hi}$ and $CD24^{+}CD61^{-}CD29^{lo}$ cells (Figure S3B).

Integrated View of Epigenetic and Gene Expression Patterns

Histone H3 lysine 4 trimethyl (H3K4me3) and H3 lysine 27 (H3K27) methylation is involved in the regulation of gene expression patterns (Bernstein et al., 2007). To investigate the relative contribution of these two types of modifications to cell-type- or developmental-stage-specific changes in gene expression in the mammary epithelium, we performed an integrated analysis of our gene expression and DNA methylation data, and recently published H3K4me3 and H3K27me3 chromatin immunoprecipitation sequencing (ChIP-seq) data for matching cell populations (Pal et al., 2013).

Although transcript levels varied between cell types, most of these changes were not associated with a change in promoter methylation or chromatin state (Figures 4A and S4A), suggesting that they play only a minor role in the transcriptional regulation of most genes involved in our system. Nonetheless, signs of epigenetic regulation were evident in a small subset of genes. We selected the transition from $CD24^{+}CD61^{+}CD29^{hi}$ cells to $CD24^{+}CD61^{+}CD29^{lo}$ cells in 9-week-old virgin mice, which showed a large range of change in expression, and for which histone mark data were available. A striking dynamic emerged when we examined histone marks in promoters of genes that were the most differentially regulated (Figure 4A, right). Genes that were downregulated showed a gain of H3K27me3 enrichment that was also sometimes punctuated by a loss of H3K4me3. A more detailed analysis of genes with the strongest decrease in expression revealed an increase in H3K27me3 methylation enrichment (Figures 4B and 4C). Among these were several genes with known roles in development and differentiation

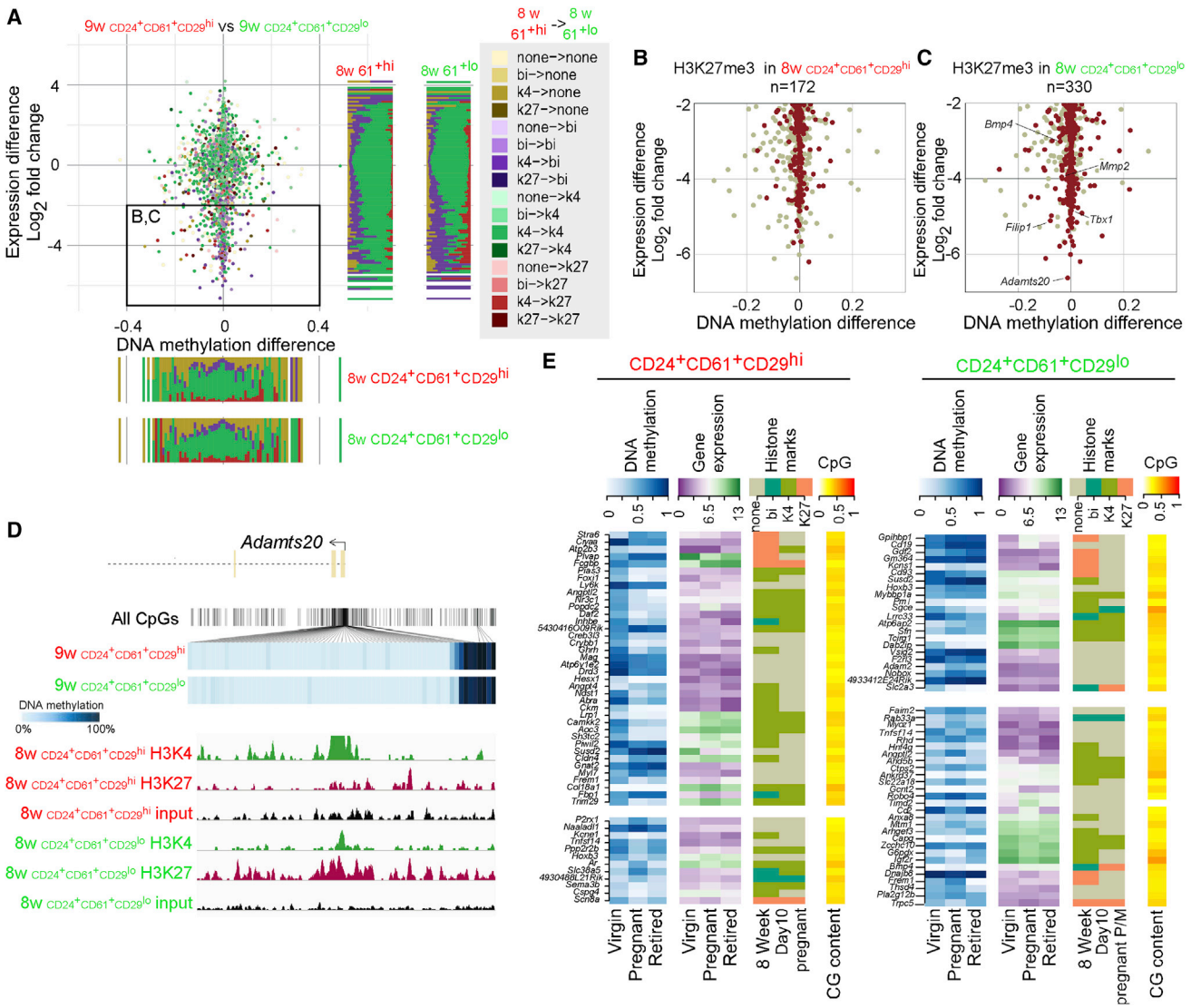

Figure 4. Integrated Analysis of Promoter DNA Methylation, Histone Modification, and Gene Expression Patterns

(A) Promoter DNA methylation and gene expression changes, comparing CD24^{+}CD61^{+}CD29^{hi} cells and CD24^{+}CD61^{+}CD29^{lo} cells in 9-week-old virgin mice. Changes in H3K4me3 and H3K27me3 enrichment are shown for each gene. The color of each point indicates the final histone state. Shades of yellow represent genes that have no histone marks in the final stage. Points colored with shades of purple had both histone marks in the final stage, whereas points colored with shades of green or red resolved to only H3K4me3 or H3K27me3 marks, respectively. The DNA methylation change (shown by the variance on the x axis) is not generally correlated with changes in expression (shown by the variance on the y axis).

(B and C) Selected set (from A, box) of loci in stem cells (B) or CD24^{+}CD61^{+}CD29^{lo} cells (C) from 8-week-old virgin mice, limited to H3K27me3 enrichment.

(D) DNA methylation and genome-browser tracks for H3K4me3 and H3K27me3 patterns for *Adamts20*, a gene that is highly expressed in stem cells from virgin mice. The transcription start site and first three exons, as well as the genomic locations of all CpGs in the promoter region, are shown. Lines are drawn from CpGs covered by RRBS to the measured methylation value. Each black bar is a CpG, the blue scale indicates the level of DNA methylation, and tracks show enrichment for the indicated histone marks. ChIP-seq read counts were normalized to sample read coverage, and enrichment is shown for CD24^{+}CD61^{+}CD29^{hi} and CD24^{+}CD61^{+}CD29^{lo} samples.

(E) DNA methylation, gene expression, enrichment for H3K4me3 and H3K27me3, and CpG density for the top 50 differentially methylated genes in CD24^{+}CD61^{+}CD29^{hi} and CD24^{+}CD61^{+}CD29^{lo}. Differentially methylated genes are sorted into two groups: the top group comprises genes that showed a greater change from the virgin stage to the pregnant state, with smaller changes between the pregnant and retired states, and the bottom group comprises genes in which the virgin state was more similar to the retired breeder state.

See also Figure S4.

(e.g., *Bmp4* and *Tbx1*). Interestingly, ADAMTS20, a secreted metalloproteinase involved in WNT and KIT signaling (Silver et al., 2008; Zhang et al., 2008), was highly expressed in $CD24^+CD61^+CD29^{hi}$ cells from virgin mice but was silenced and H3K27me3-enriched in $CD24^+CD61^+CD29^{lo}$ cells (Figure 4D). The 181 gene promoters that gained H3K27me3 methylation in $CD24^+CD61^+CD29^{lo}$ cells but were not marked in $CD24^+CD61^+CD29^{hi}$ cells were mostly enriched in developmental processes and cell migration (Figure S4B).

We next analyzed associations among DNA methylation, expression, histone marks, and CpG density for the top 50 genes that showed differential DNA methylation in $CD24^+CD61^+CD29^{hi}$ and $CD24^+CD61^+CD29^{lo}$ cells. These differentially methylated genes were sorted into two groups: (1) genes that showed a greater change from the virgin state to the pregnant state, with smaller changes between the pregnant and retired states; and (2) genes in which the virgin state was more similar to the retired state. Several genes such as *Ar* and *Lrp1* in $CD24^+CD61^+CD29^{hi}$ cells and *Capg* and *Tcrg1* in $CD24^+CD61^+CD29^{lo}$ cells showed uniform high expression and H3K4me3 enrichment in all stages, implying essential roles throughout life (Figure 4E).

To search for transcription networks that may be affected by changes in DNA methylation and histone modification patterns, we analyzed the promoter methylation of TFs that were differentially expressed between virgin and retired breeder mice. *Foxi1* showed the most dynamic changes in expression and DNA methylation among both cell types and developmental stages, with the highest expression in $CD24^+CD61^+CD29^{hi}$ cells from 3-week-old virgin mice (Figure S4C). *Foxi1* was also one of the few TFs that were upregulated by AzaC and VPA treatment in pregnant mice (Figure S3A), further supporting its epigenetic regulation. *Cldn4*, encoding a tight junction protein, showed the highest expression and lowest methylation in $CD24^+CD61^-CD29^{lo}$ cells (Figure 5A). It was also among the most significantly upregulated genes by AzaC treatment (Figure S3), suggesting that its expression is at least in part regulated by DNA methylation. Thus, we investigated the expression and localization of CLDN4 by immunofluorescence in combination with that of CD61/ITGB3, a cell-surface marker that is used to identify $CD24^+CD61^+CD29^{hi}$ and $CD24^+CD61^+CD29^{lo}$ cells. In 9-week-old virgin control mice, CLDN4 was localized between luminal epithelial cells, whereas CD61 was only seen in the basal layer that is in contact with the basement membrane (Figure 5B). However, in AzaC-treated mice and, even more remarkably, in 9-week-old $Dnmt1^{+/chip}$ mice, the localization of both CLDN4 and CD61 was altered and they displayed a significant overlap (Figure 5B), although the frequency of $CD61^+$ cells did not change. These results further support the regulation of *Cldn4* expression by DNA methylation.

Key Roles for p27 and TGFβ Signaling in Mammary Epithelial Progenitors

Our molecular profiling demonstrated that pregnancy has the most pronounced effect on $CD24^+CD61^+CD29^{hi}$ and $CD24^+CD61^+CD29^{lo}$ cells (Figures 2B and 2C). We identified focal adhesion and the TGFβ signaling pathway as being more highly activated in $CD24^+CD61^+CD29^{lo}$ cells from 9-week-old virgin mice compared with mice in other stages (Figure 6A). In our related studies in human breast, we also identified the TGFβ signaling pathway and p27 (*Cdkn1b*) as being the most significantly altered by parity and as key regulators of mammary epithelial progenitor cell proliferation (Choudhury et al., 2013). To further investigate the evolutionary conservation of these findings, we analyzed the expression of p27 and members of the TGFβ signaling pathway in our gene expression data. Expression of p27 was highest in $CD24^+CD61^+CD29^{hi}$ and $CD24^+CD61^+CD29^{lo}$ cells from 9-week-old mice, and much lower levels were observed in other reproductive stages and in $CD24^+CD61^-CD29^{lo}$ cells (Figures 6B and S5). Since the expression of p27 is commonly regulated at the protein level, we performed immunoblot analysis of purified cell populations from virgin and retired breeder mice, which showed higher p27 protein levels in $CD24^+CD61^+CD29^{lo}$ cells from 9-week-old virgin mice (Figure 6C). To analyze the expression of p27 and the localization of $p27^+$ cells in intact mammary tissues, we performed immunofluorescence in combination with CD61. This analysis showed high expression of p27 in $CD61^+$ cells in 9-week-old and even 24-week-old virgin mice, whereas no such cells were detected in retired breeders (Figure 6D and S5A).

To investigate whether decreased TGFβ levels might influence the frequency of $p27^+$ cells, we performed an immunofluorescence analysis of p27 and CD61 in mammary glands from virgin $Tgfb1^{+/+}$ and $Tgfb1^{+/-}$ (Ewan et al., 2002, 2005) and mammary epithelium-specific *Tgfbr2* knockout (Forrester et al., 2005) mice. We found a higher frequency of $p27^+$ cells in both $Tgfb1^{+/-}$ and older (21- to 29-week-old) $Tgfbr2^{-/-}$ mice (Figures 6E and 6F), implying an expansion of the $CD24^+CD61^+CD29^{lo}$ cell pool with proliferative capacity due to decreased TGFβ signaling. However, none of these differences reached statistical significance.

To address the regulation of $p27^+$ progenitors by hormonal and TGFβ signaling more directly, we established a mammary gland explant culture model. The use of explant cultures in which the tissue remains intact has the advantage that the cells remain in their intact microenvironment. Several recent studies have demonstrated that the

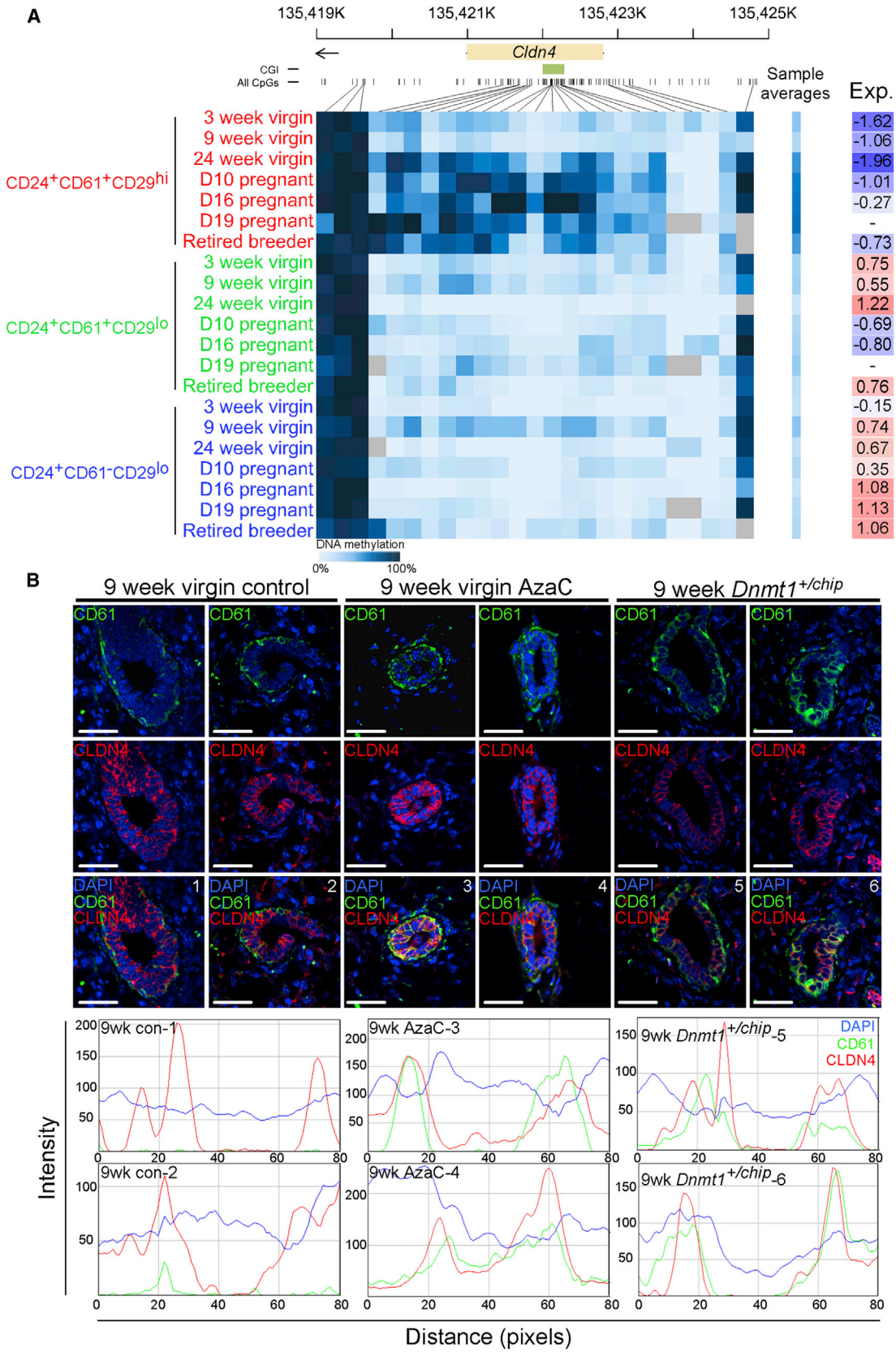

(legend on next page)

dissociation of the cells and cell culture by itself increases the progenitor potential of mammary epithelial cells and may also shift them to a more myoepithelial lineage (Prater et al., 2014; Stingl, 2009). We used this explant model to analyze the frequencies of $p27^+$ and proliferating ($Ki67^+$ or $BrdU^+$) cells after treatment with ovarian hormones mimicking different phases of the estrus/menstrual cycle in the presence or absence of a TGFBR kinase inhibitor (LY2109761). The frequency of $p27^+$ cells was higher in the mammary tissue of 9-week-old virgins compared with retired breeders, was inversely correlated with that of $Ki67^+$ and $BrdU^+$ cells, and was decreased after TGFBR kinase inhibitor (TGFBRi) treatment (Figures 6G–6I and S5B). In tissues from retired breeders TGFBRi and hormonal treatment did not induce any significant changes, due to the very low basal levels of $p27^+$ and $BrdU^+$ cells. These results suggest a high degree of conservation in the regulation of hormone-responsive mammary epithelial progenitors by parity between mice and humans (Choudhury et al., 2013), and key roles for p27 and TGFβ signaling in this process.

DISCUSSION

Our comprehensive gene expression and DNA methylation profiles covering multiple cell types in normal mammary gland from mice of different ages and reproductive stages provide a rich resource for future investigations of the way in which age- and pregnancy-induced DNA methylation alters $CD24^+CD61^+CD29^{hi}$ and $CD24^+CD61^+CD29^{lo}$ cells, potentially restricting their hormone responsiveness and proliferative capacity, which may contribute to the decreased susceptibility of parous mice to mammary tumorigenesis (Russo et al., 2005, 2006a, 2006b). Through our analyses, we found that pregnancy has the most pronounced effect on $CD24^+CD61^+CD29^{hi}$ and $CD24^+CD61^+CD29^{lo}$ cells, and many of the differences relate to the downregulation of genes and pathways that are important for stem cell function, including Hedgehog and TGFβ signaling.

The expression profiles of the three distinct cell populations show a high correlation in 3-week-old virgin mice, which represents the prepubertal immature mammary gland, but become very distinct with puberty and even more so during pregnancy, whereas cells from retired breeders resemble those from mice in prepregnant virgin states. These results suggest that the transcriptome and the phenotype of mammary epithelial cells are mostly influenced by reproductive hormones (Asselin-Labat et al., 2010). We identified several TFs with expression restricted to $CD24^+CD61^+CD29^{hi}$ cells, many of which belong to the *Id*, *Snai*, and *Foxo* gene families. All of these gene families are targets of TGFβ signaling and have known roles in stem cells (Eijkelenboom and Burgering, 2013; Ruzinova and Benezra, 2003). Some of these TFs were expressed in $CD24^+CD61^+CD29^{hi}$ cells regardless of age or reproductive stage (e.g., *Id4* and *Snai2*), implying that they play key roles in stem cell function, whereas others were only present in prepubertal virgin (e.g., *Snai1*) or retired breeder (e.g., *Foxd3*) mice, potentially reflecting stage-specific function.

In contrast to the significant cell-type- and reproductive-stage-specific differences in gene expression profiles, the DNA methylation and histone modification (H3K27me3) patterns showed much less pronounced changes. For the majority of differentially expressed genes, alterations in mRNA levels were not associated with changes in DNA methylation or enrichment for the H3K27me3 mark. These findings are consistent with results of studies that investigated the DNA methylation profiles of a wide array of cell types in both mice and humans (Bock et al., 2012; Ziller et al., 2013), and with the relatively minor effects of *Ezh2* deletion on mammary epithelial cell differentiation (Michalak et al., 2013; Pal et al., 2013). A few TFs (e.g., *Trp73* and *Foxi1*) displayed both differential DNA methylation and expression among cell types or across stages, and *Foxi1* expression was also induced by AzaC and VPA treatment. As none of these TFs have been analyzed in the mammary gland, the physiologic relevance of their expression and epigenetic patterns is still unclear. However, their function in other organs suggests potential roles in mammary epithelial stem or progenitor cells.

$CD24^+CD61^+CD29^{hi}$ cells formed the most distinct category in both the gene expression and DNA methylation profiles. Whereas expression profiles separated $CD24^+CD61^+CD29^{hi}$ cells from all ages and reproductive stages into a unique group, clustering based on DNA methylation levels suggested that age and pregnancy

Figure 5. CLDN4 Expression and DNA Methylation Patterns in Mammary Epithelial Cells

(A) Degree of *Cldn4* DNA methylation and gene expression. The transcription start site and gene (single exon), as well as all CpGs along the genomic coordinates, are shown. Lines are drawn from CpGs covered by RRBS to a column showing the methylation state of that CpG in each sample. Sample methylation averages and normalized expression values are shown to the right of the image.

(B) Top: representative multicolor immunofluorescence analysis of CLDN4 (red) and CD61 (green) expression in mammary glands from the indicated treatment groups. Nuclei are visualized by DAPI (blue) stain. Scale bar, 25 μm. Bottom: RGB spectra demonstrating the overlap between CD61 and CLDN4.

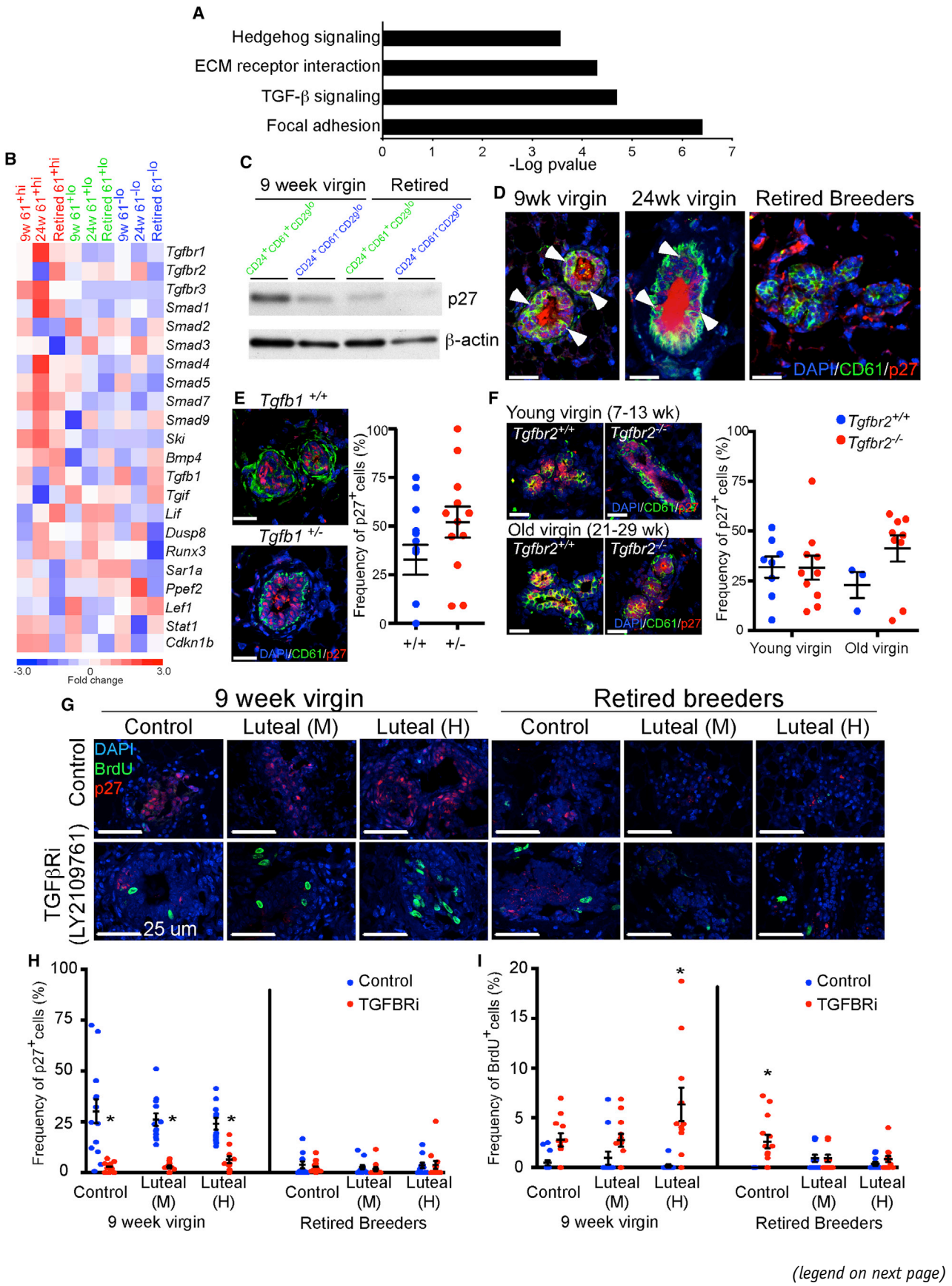

(legend on next page)

induce unique changes in the DNA methylation profiles of $CD24^+CD61^+CD29^{hi}$ cells, which then may alter their self-renewal and differentiation capacity. As proliferative (i.e., stem and progenitor) cells are thought to be the cellular targets of neoplastic transformation, investigating these DNA methylation changes in further detail may reveal markers relevant to breast cancer risk. Related to this, our finding that p27 and TGFβ signaling show the most significant differential expression and activity between $CD24^+CD61^+CD29^{lo}$ cells from 9-week-old virgin and retired breeder mice correlates with our recent results describing the association of these genes with breast cancer risk in women (Choudhury et al., 2013).

In summary, our data support the hypothesis that pregnancy induces permanent changes in $CD24^+CD61^+CD29^{hi}$ and $CD24^+CD61^+CD29^{lo}$ cells that are relevant to breast cancer risk, and imply that depletion of these cells may be a feasible cancer prevention strategy. Since studies in mice appear to reproduce our findings in women, they may provide a physiologically relevant preclinical model in which to test the feasibility of such a strategy.

EXPERIMENTAL PROCEDURES

Mice

We purchased 3-, 9-, and 24-week-old virgin; D10, D16, and D19 timed pregnant; and retired breeder C57BL6 female mice from Charles River Laboratories (Wilmington, MA) and The Jackson Laboratory (Bar Harbor, ME). All animal experiments were conducted by trained personnel and followed protocols approved by the Dana-Farber Cancer Institute and Harvard Medical School Animal Care and Use Committees. For inhibitor treatment experiments, 125–250 ng/g of AzaC and 100–300 μg/g (weight of mouse) of VPA were dissolved in 150–300 μl PBS and delivered by intraperitoneal injections (Figure S1A). Control mice received PBS only. *Dnmt1*$^{+/chip}$ mice (Gaudet et al., 2003) were bred and maintained in Boston Children's Hospital according to procedures approved by the IACUC.

Histology, Immunohistochemistry, and Immunofluorescence Analyses

Histology, immunohistochemical staining, and multicolor immunofluorescence analysis for BrdU, Ki67, p27, CD61, and CLDN4 (Life Technologies) were performed as previously described (Choudhury et al., 2013). Whole-mount mouse mammary glands were fixed in Carnoy's solution and stained with carmine. Samples were imaged on a Nikon Ti/E inverted microscope using Nikon Elements software.

For further details regarding the materials and methods used in this work, see Supplemental Experimental Procedures.

ACCESSION NUMBERS

The raw data files and details regarding the methods reported in this work have been deposited in the Gene Expression Omnibus under accession number GSE54150.

SUPPLEMENTAL INFORMATION

Supplemental Information includes Supplemental Experimental Procedures, six figures, and seven tables and can be found with this article online at http://dx.doi.org/10.1016/j.stemcr.2014.12.009.

Figure 6. Cell-, Age-, and Reproductive-Stage-Specific Expression of p27 and Its Regulation by TGFβ Signaling

(A) Signaling pathways significantly enriched in genes differentially expressed in $CD24^+CD61^+CD29^{lo}$ cells between 9-week-old virgin and retired breeder mice.

(B) Heatmap depicting the expression of genes related to TGFβ signaling in $CD24^+CD61^+CD29^{hi}$ and $CD24^+CD61^+CD29^{lo}$ from 9- and 24-week-old virgin and retired breeder mice.

(C) Immunoblot analysis of p27 protein levels in $CD24^+CD61^+CD29^{lo}$ and $CD24^+CD61^-CD29^{lo}$ cells from 9-week-old virgin and retired breeder mice.

(D) Multicolor immunofluorescence analysis of p27 (red) and CD61 (green) expression in mammary glands from 9-week-old virgin and retired breeder mice. Nuclei are visualized by DAPI (blue) stain. White arrows indicate $p27^+CD61^+$ progenitors in mammary glands of 9-week-old virgin mice. Scale bar, 25 μm.

(E) Left: multicolor immunofluorescence analysis of p27 (red) and CD61 (green) expression in mammary glands from *Tgfb1*$^{+/+}$ and *Tgfb1*$^{+/-}$ mice. Nuclei are visualized by DAPI (blue) stain. Right: graph depicting quantification of the frequency of $p27^+$ cells. Error bars represent median ± SEM.

(F) Left: multicolor immunofluorescence analysis of p27 (red) and CD61 (green) expression in mammary glands from *Tgfbr2*$^{+/+}$ and *Tgfbr2*$^{-/-}$ mice. Nuclei are visualized by DAPI (blue) stain. Right: graph depicting quantification of the frequency of $p27^+$ cells. Error bars represent median ± SEM.

(G) Multicolor immunofluorescence analysis of p27 and BrdU expression in tissue slices from mammary glands of 9-week-old virgin and retired breeder mice untreated or treated with TGFBRi and ovarian hormones mimicking the luteal phase in mouse (M) and human (H). Nuclei are visualized by DAPI (blue) stain. Scale bar, 25 μm.

(H and I) Frequency of $p27^+$ (H) and $BrdU^+$ (I) cells in tissue slices from three to five independent cases treated with TGFb receptor inhibitor (TGFBRi) and ovarian hormones mimicking the luteal phase in mouse (M) and human (H). Asterisks (*) indicate significant difference ($p < 0.05$, multiple t tests). Error bars represent median ± SEM.

See also Figure S5.

AUTHOR CONTRIBUTIONS

S.J.H. designed and performed the experiments and data analysis. K.C. performed bioinformatics analysis of the data. D.J., A. Merlini, S.C., and R.M. assisted with the experiments and data analysis. R.Y., F.A.R., and L.J.-G. provided the *Dnmt1*$^{+/+}$ and *Dnmt1*$^{+/chip}$ mice. A.C. and H.L.M. provided the mammary gland sections for the *Tgfbr2*$^{+/+}$ and *Tgfbr2*$^{-/-}$ mice. P.B. prepared the RRBS libraries. M.H.B.-H. provided the mammary gland sections for the *Tgfb1*$^{+/+}$ and *Tgfb1*$^{+/-}$ mice. A. Meissner and K.P. supervised the study. All authors contributed with discussions and wrote the manuscript.

ACKNOWLEDGMENTS

We thank the staffs of the Dana-Farber Cancer Institute Flow Cytometry Core Facilities, Molecular Biology Core Facilities, and Confocal and Light Microscopy Core Facilities for their outstanding services and technical support. This work was supported by the National Cancer Institute (F32 CA156991 to S.J.H. and P01 CA080111 to K.P.), the Giovanni Armenise-Harvard Foundation Summer Fellowship Program (A. Merlini), the Susan G. Komen Foundation (R.M.), the Terri Brodeur Foundation (S.C.), the New York Stem Cell Foundation (A. Meissner), and U.S. Army Congressionally Directed Research (W81XWH-07-1-0294 to K.P.). A. Meissner is a New York Stem Cell Foundation–Robertson Investigator. This article is dedicated to the memory of Dr. Edward Fox.

Received: January 10, 2014
Revised: December 16, 2014
Accepted: December 16, 2014
Published: January 22, 2015

REFERENCES

Asselin-Labat, M.L., Sutherland, K.D., Barker, H., Thomas, R., Shackleton, M., Forrest, N.C., Hartley, L., Robb, L., Grosveld, F.G., van der Wees, J., et al. (2007). Gata-3 is an essential regulator of mammary-gland morphogenesis and luminal-cell differentiation. Nat. Cell Biol. *9*, 201–209.

Asselin-Labat, M.L., Vaillant, F., Sheridan, J.M., Pal, B., Wu, D., Simpson, E.R., Yasuda, H., Smyth, G.K., Martin, T.J., Lindeman, G.J., and Visvader, J.E. (2010). Control of mammary stem cell function by steroid hormone signalling. Nature *465*, 798–802.

Beerman, I., Bock, C., Garrison, B.S., Smith, Z.D., Gu, H., Meissner, A., and Rossi, D.J. (2013). Proliferation-dependent alterations of the DNA methylation landscape underlie hematopoietic stem cell aging. Cell Stem Cell *12*, 413–425.

Bernstein, B.E., Meissner, A., and Lander, E.S. (2007). The mammalian epigenome. Cell *128*, 669–681.

Bock, C., Beerman, I., Lien, W.H., Smith, Z.D., Gu, H., Boyle, P., Gnirke, A., Fuchs, E., Rossi, D.J., and Meissner, A. (2012). DNA methylation dynamics during in vivo differentiation of blood and skin stem cells. Mol. Cell *47*, 633–647.

Boyle, P., Clement, K., Gu, H., Smith, Z.D., Ziller, M., Fostel, J.L., Holmes, L., Meldrim, J., Kelley, F., Gnirke, A., and Meissner, A. (2012). Gel-free multiplexed reduced representation bisulfite sequencing for large-scale DNA methylation profiling. Genome Biol. *13*, R92.

Choudhury, S., Almendro, V., Merino, V.F., Wu, Z., Maruyama, R., Su, Y., Martins, F.C., Fackler, M.J., Bessarabova, M., Kowalczyk, A., et al. (2013). Molecular profiling of human mammary gland links breast cancer risk to a p27(+) cell population with progenitor characteristics. Cell Stem Cell *13*, 117–130.

Desgrosellier, J.S., Lesperance, J., Seguin, L., Gozo, M., Kato, S., Franovic, A., Yebra, M., Shattil, S.J., and Cheresh, D.A. (2014). Integrin αvβ3 drives slug activation and stemness in the pregnant and neoplastic mammary gland. Dev. Cell *30*, 295–308.

Eijkelenboom, A., and Burgering, B.M. (2013). FOXOs: signalling integrators for homeostasis maintenance. Nat. Rev. Mol. Cell Biol. *14*, 83–97.

Ewan, K.B., Shyamala, G., Ravani, S.A., Tang, Y., Akhurst, R., Wakefield, L., and Barcellos-Hoff, M.H. (2002). Latent transforming growth factor-beta activation in mammary gland: regulation by ovarian hormones affects ductal and alveolar proliferation. Am. J. Pathol. *160*, 2081–2093.

Ewan, K.B., Oketch-Rabah, H.A., Ravani, S.A., Shyamala, G., Moses, H.L., and Barcellos-Hoff, M.H. (2005). Proliferation of estrogen receptor-alpha-positive mammary epithelial cells is restrained by transforming growth factor-beta1 in adult mice. Am. J. Pathol. *167*, 409–417.

Forrester, E., Chytil, A., Bierie, B., Aakre, M., Gorska, A.E., Sharif-Afshar, A.R., Muller, W.J., and Moses, H.L. (2005). Effect of conditional knockout of the type II TGF-beta receptor gene in mammary epithelia on mammary gland development and polyomavirus middle T antigen induced tumor formation and metastasis. Cancer Res. *65*, 2296–2302.

Gaudet, F., Hodgson, J.G., Eden, A., Jackson-Grusby, L., Dausman, J., Gray, J.W., Leonhardt, H., and Jaenisch, R. (2003). Induction of tumors in mice by genomic hypomethylation. Science *300*, 489–492.

Gu, B., Watanabe, K., Sun, P., Fallahi, M., and Dai, X. (2013). Chromatin effector Pygo2 mediates Wnt-notch crosstalk to suppress luminal/alveolar potential of mammary stem and basal cells. Cell Stem Cell *13*, 48–61.

Guo, W., Keckesova, Z., Donaher, J.L., Shibue, T., Tischler, V., Reinhardt, F., Itzkovitz, S., Noske, A., Zürrer-Härdi, U., Bell, G., et al. (2012). Slug and Sox9 cooperatively determine the mammary stem cell state. Cell *148*, 1015–1028.

Hanna, L.A., Foreman, R.K., Tarasenko, I.A., Kessler, D.S., and Labosky, P.A. (2002). Requirement for Foxd3 in maintaining pluripotent cells of the early mouse embryo. Genes Dev. *16*, 2650–2661.

Hennighausen, L., and Robinson, G.W. (2005). Information networks in the mammary gland. Nat. Rev. Mol. Cell Biol. *6*, 715–725.

Kramerov, D.A., and Vassetzky, N.S. (2005). Short retroposons in eukaryotic genomes. Int. Rev. Cytol. *247*, 165–221.

Li, Q., Zhu, F., and Chen, P. (2012). miR-7 and miR-218 epigenetically control tumor suppressor genes RASSF1A and Claudin-6 by targeting HoxB3 in breast cancer. Biochem. Biophys. Res. Commun. *424*, 28–33.

Michalak, E.M., Nacerddine, K., Pietersen, A., Beuger, V., Pawlitzky, I., Cornelissen-Steijger, P., Wientjens, E., Tanger, E., Seibler, J., van Lohuizen, M., and Jonkers, J. (2013). Polycomb group gene Ezh2

regulates mammary gland morphogenesis and maintains the luminal progenitor pool. Stem Cells *31*, 1910–1920.

Pal, B., Bouras, T., Shi, W., Vaillant, F., Sheridan, J.M., Fu, N., Breslin, K., Jiang, K., Ritchie, M.E., Young, M., et al. (2013). Global changes in the mammary epigenome are induced by hormonal cues and coordinated by Ezh2. Cell Rep. *3*, 411–426.

Prater, M.D., Petit, V., Alasdair Russell, I., Giraddi, R.R., Shehata, M., Menon, S., Schulte, R., Kalajzic, I., Rath, N., Olson, M.F., et al. (2014). Mammary stem cells have myoepithelial cell properties. Nat. Cell Biol. *16*, 942–950, 1–7.

Rios, A.C., Fu, N.Y., Lindeman, G.J., and Visvader, J.E. (2014). In situ identification of bipotent stem cells in the mammary gland. Nature *506*, 322–327.

Russo, J., Mailo, D., Hu, Y.F., Balogh, G., Sheriff, F., and Russo, I.H. (2005). Breast differentiation and its implication in cancer prevention. Clin. Cancer Res. *11*, 931s–936s.

Russo, J., Balogh, G.A., Chen, J., Fernandez, S.V., Fernbaugh, R., Heulings, R., Mailo, D.A., Moral, R., Russo, P.A., Sheriff, F., et al. (2006a). The concept of stem cell in the mammary gland and its implication in morphogenesis, cancer and prevention. Front. Biosci. *11*, 151–172.

Russo, J., Balogh, G.A., Heulings, R., Mailo, D.A., Moral, R., Russo, P.A., Sheriff, F., Vanegas, J., and Russo, I.H. (2006b). Molecular basis of pregnancy-induced breast cancer protection. Eur. J. Cancer Prev. *15*, 306–342.

Ruzinova, M.B., and Benezra, R. (2003). Id proteins in development, cell cycle and cancer. Trends Cell Biol. *13*, 410–418.

Shackleton, M., Vaillant, F., Simpson, K.J., Stingl, J., Smyth, G.K., Asselin-Labat, M.L., Wu, L., Lindeman, G.J., and Visvader, J.E. (2006). Generation of a functional mammary gland from a single stem cell. Nature *439*, 84–88.

Silver, D.L., Hou, L., Somerville, R., Young, M.E., Apte, S.S., and Pavan, W.J. (2008). The secreted metalloprotease ADAMTS20 is required for melanoblast survival. PLoS Genet. *4*, e1000003.

Smith, Z.D., and Meissner, A. (2013). DNA methylation: roles in mammalian development. Nat. Rev. Genet. *14*, 204–220.

Spike, B.T., Engle, D.D., Lin, J.C., Cheung, S.K., La, J., and Wahl, G.M. (2012). A mammary stem cell population identified and characterized in late embryogenesis reveals similarities to human breast cancer. Cell Stem Cell *10*, 183–197.

Stingl, J. (2009). Detection and analysis of mammary gland stem cells. J. Pathol. *217*, 229–241.

Tiffen, J.C., Bailey, C.G., Marshall, A.D., Metierre, C., Feng, Y., Wang, Q., Watson, S.L., Holst, J., and Rasko, J.E. (2013). The cancer-testis antigen BORIS phenocopies the tumor suppressor CTCF in normal and neoplastic cells. Int. J. Cancer *133*, 1603–1613.

Tou, L., Liu, Q., and Shivdasani, R.A. (2004). Regulation of mammalian epithelial differentiation and intestine development by class I histone deacetylases. Mol. Cell. Biol. *24*, 3132–3139.

van Amerongen, R., Bowman, A.N., and Nusse, R. (2012). Developmental stage and time dictate the fate of Wnt/β-catenin-responsive stem cells in the mammary gland. Cell Stem Cell *11*, 387–400.

Van Keymeulen, A., Rocha, A.S., Ousset, M., Beck, B., Bouvencourt, G., Rock, J., Sharma, N., Dekoninck, S., and Blanpain, C. (2011). Distinct stem cells contribute to mammary gland development and maintenance. Nature *479*, 189–193.

Zhang, Y., Andl, T., Yang, S.H., Teta, M., Liu, F., Seykora, J.T., Tobias, J.W., Piccolo, S., Schmidt-Ullrich, R., Nagy, A., et al. (2008). Activation of beta-catenin signaling programs embryonic epidermis to hair follicle fate. Development *135*, 2161–2172.

Ziller, M.J., Gu, H., Müller, F., Donaghey, J., Tsai, L.T., Kohlbacher, O., De Jager, P.L., Rosen, E.D., Bennett, D.A., Bernstein, B.E., et al. (2013). Charting a dynamic DNA methylation landscape of the human genome. Nature *500*, 477–481.